Electromagnetic wave absorption properties of polymer-derived SiCN ceramics doped with Co_3C particles

S. WANG[a,b], H. Y. GONG[a,b,*], Y. J. ZHANG[a,b], M. Z. ASHFAQ[a,b], J. JING[a,b]
[a]*Key Laboratory for Liquid-Solid Structural Evolution & Processing of Materials Ministry of Education, Shandong University, Jinan 250061, P. R. China*
[b]*Key Laboratory of Special Functional Aggregated Materials, Ministry of Education, Shandong University, Jinan 250061, P. R. China*

SiCN ceramics doped with magnetic particles Co_3C were prepared by polymer derivatization. On this basis, the composition and microstructures of SiCN based composite ceramics pyrolyzed at different temperatures were studied. The electromagnetic parameters and the electromagnetic wave absorption performance at 2-18 GHz were analyzed. The results show that there was a minimum reflection loss (R_{Lmin}) value of -14 dB at 16.5GHz and an effective absorption bandwidth (R_L<-10dB) of 0.6 GHz when the pyrolysis temperature was 1300 ℃ and the sample thickness was 2 mm. This indicates that SiCN ceramics doped with Co_3C particles can be a potential candidate in the field of electromagnetic wave absorbing materials.

(Received June 3, 2020; accepted November 25, 2020)

Keywords: Co_3C, SiCN ceramics doped with Co_3C particles, Different pyrolysis temperatures, Electromagnetic wave absorption properties

1. Introduction

Nowadays, critical pollution problems of electromagnetic waves (EMW) have been induced due to the speedy development of the network, radar detection technology, wireless communication technology, and so on. EMW pollution to be solved on account of EM not only brings harm to human body, but also interferes electronic equipment, and even poses potential threats to the military safety of a country [1-4]. In this regard, it is an important strategy to study efficient EMW absorbing materials to solve the above problem. Absorbing materials can be divided into two categories: absorbing and interfering materials. The interfering mechanism is that the incident EMW and the reflected EMW can interfere and cancel each other on the surface of the material, thus consuming the electromagnetic energy. The absorbing mechanism mainly refers to the energy of electromagnetic wave incident into the material is converted into heat energy or other forms of energy, and then dissipated. Basic conditions of attenuating EMW by absorbing materials are shown as following: When the EMW is incident on the surface of the sample, it enters the material as far as possible without reflection and can be attenuated to the maximum extent inside the material. That is to say, EMW absorbing materials should meet the following principles [5,6]: (1) Impedance Matching Principle: The impedance of the material is matched with that of the air, so that EMW can enter the absorbing material to the greatest extent. (2) Attenuation Principle: After EMW enters the material, its energy can be attenuated rapidly.

In order to prepare materials with efficient EMW absorbing properties, SiCN ceramics were used as matrix materials in this study. SiCN ceramics with unique amorphous structure, homogeneous chemical composition, high temperature resistance and excellent dielectric properties [7] are considered as potential candidates for the EMW absorption material matrix. However, the impedance matching with air is unsatisfactory because SiCN ceramics only possess the dielectric loss performance, but have no magnetic energy loss performance, which limits its application in the special environment. Therefore, in the current reports, many researches have focused on dispersing magnetic particles (such as Fe, Ni) or their compounds or rare earth oxides into the SiCN ceramic matrix, in order to synthesize the electromagnetic performance of composite materials and obtain improved absorbing properties. For instance, SiCN(Fe) [8], SiCN(Ni) [9], rare earth oxides doped SiCN (Fe) composite ceramics [10] and europium-doped SiCN(Fe) composite ceramics [11] have been synthesized by the polymer-derived method. The above composites have excellent EMW absorption properties, which benefit from the combination of the dielectric loss effect of SiCN ceramics and the magnetic energy loss function of the magnetic phase.

Cobalt and its compounds have great potential applications in EMW absorbing materials due to their high permeability and electric polarization loss ability [12-14]. Previous studies have introduced cobalt or its compounds into the carbon matrix material so as to gain the composite materials with improved EMW absorption properties. For

example, Zhang et al. [15] studied the Co/C nanofiber composite by the electrospinning technique. Qi et al. [16] prepared Co@C nanotubes-graphene ternary hybrids by catalytic decomposition of Co_3O_4/reduced graphene oxide (Co_3O_4/RGO) with acetylene. Abdalla et al. [17] prepared the Co_3O_4/C composite nanofibrous membrane, which not only has good magnetic properties, but also has excellent EMW absorption properties.

In this study, cobalt acetylacetonate ($Co(acac)_3$) was used as one of the raw materials. By using $Co(acac)_3$ as the magnetic particle source and mixing it with liquid polysilazane (PSZ), the magnetic particles Co_3C can be formed in situ in the SiCN ceramic matrix after the mixture was crosslinked and pyrolyzed. The magnetic particles generated in situ were more uniformly dispersed as compared to the magnetic particles directly mixed into the matrix mechanically [18]. In addition, the SiCN ceramics doped with Co_3C particles prepared in this study have more excellent EMW absorption properties (R_{Lmin}= -14 dB, 2 mm) as compared to the SiCN(Fe) composite ceramics (R_{Lmin}= -10.9 dB, 4 mm)[8] and rare earth oxide (Dy_2O_3, Sm_2O_3, Y_2O_3, Gd_2O_3, Eu_2O_3) doped SiCN(Fe) ceramics ($R_{Lmin}\geq$-12 dB, 2 mm)[10,11]. This may be attributed to that SiCN ceramics doped with Co_3C particles have better magnetic energy loss capacity than SiCN(Fe) and rare earth oxide doped SiCN(Fe) ceramic: When the iron content was 50wt%, the magnetic loss tangent ($\tan\delta_\mu$) of SiCN(Fe) was less than 0.5[8]; When the iron content was 5wt% and the rare earth oxide content was 5-45wt%, the $\tan\delta_\mu$ of rare earth oxide doped SiCN(Fe) ceramic was less than 0.5[10,11]; The maximum $\tan\delta_\mu$ of SiCN ceramics doped with Co_3C particles prepared in this study can reach 0.7 when the content of cobalt element was 10wt%, through which we speculate that the excellent magnetic energy loss ability is one of the reasons why SiCN ceramics doped with Co_3C particles have better EMW absorbing performance compared to SiCN(Fe) and rare earth oxide doped SiCN(Fe) ceramic. In a word, this study provides a new strategy for improving the EMW absorption performance of SiCN based composite ceramics.

2. Experiment

2.1. Experimental raw materials and reagents

Liquid polysilazane (PSZ) for experimental use was provided by Shanghai Haiyi Science and Technology Co., Ltd. of China, cobalt acetylacetonate ($Co(acac)_3$) powder (99.9%, 50 nm) was provided by Shanghai Macklin Co., Ltd. of China, and inert gas (nitrogen) was provided by Jinan Deyang Gas Co., Ltd. of China.

2.2. Experimental procedure

The $Co(acac)_3$ was mixed with PSZ at a certain ratio (the mass ratio of cobalt was 10wt%). The mixture was placed in the double pipe gas distribution system, and then stirred for 1 hour under nitrogen atmosphere. The liquid mixture uniformly stirred was placed in a tubular furnace and crosslinked for 2 hours under nitrogen atmosphere at 600 ℃. The crosslinked precursor powder was milled and passed through the 200-mesh sieve. The adhesive was added to the obtained powder, which was ground evenly and then pressed into discoid tablets with a thickness of about 2 mm. Ceramics were synthesized by pyrolysis of tablets in a tubular furnace for 2 hours at different temperatures (1000 ℃, 1100 ℃, 1200 ℃, 1300 ℃, 1400 ℃, 1500 ℃). Next, the ceramics were ground into powder and mixed with paraffin (the mass ratio of ceramic to paraffin was 5:2), and pressed into rings with inner diameter of 3.04 mm and outer diameter of 6.9 mm to test their electromagnetic parameters.

2.3. Characterization

The fracture morphology of the samples was analyzed by the SU-70 scanning electron microscopy (SEM) of Hitachi Company, Japan. The qualitative chemical composition analysis was carried out for the material fracture surface by Genesis energy spectrum analyzer with SEM. The X-ray diffraction analysis was made for samples by X'Pert PRO multipurpose powder X-ray diffractometer produced in Panaco, Netherlands. The crystal state of carbon in samples was analyzed by LabRam-1B confocal micro-Raman spectrometer made by Jobinyvon, France. The magnetic properties of the samples were tested by JDAW-2000D vibrating sample magnetometer produced by Yingpu, China. The electromagnetic parameters of samples were measured by E5071C ENA network analyzer produced by Keysight, USA.

3. Results and discussion

3.1. Phase composition

Fig. 1(a) shows the XRD spectra of the precursor powder crosslinked for 2 hours at 600 ℃. The obvious diffraction peaks at 44.2, 51.5 and 75.9° can be indexed to Co with a cubic structure (JCPDS No. 15-0806). This indicates that cobalt was reduced from $Co(acac)_3$ during crosslinking. There were no other diffraction peaks except cobalt, which indicates that all phases are amorphous except the element cobalt.

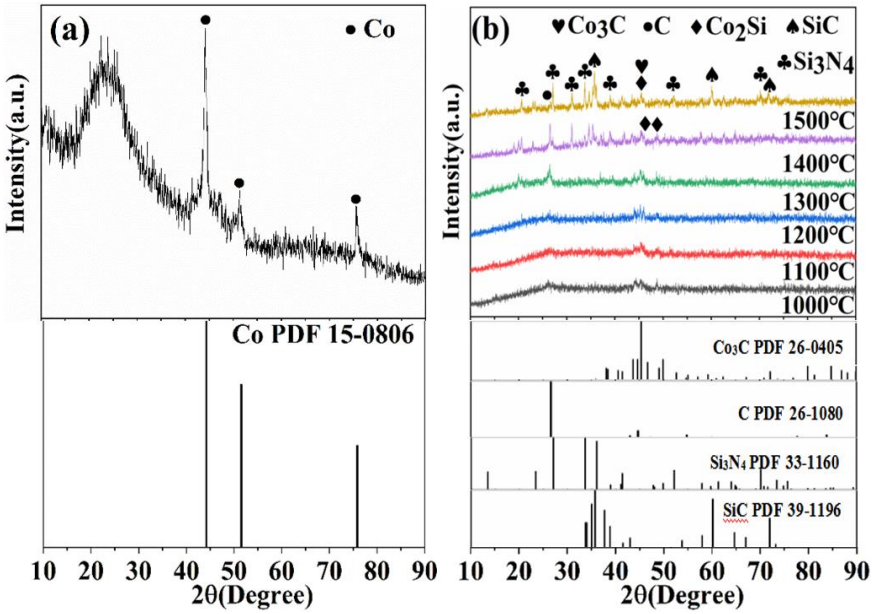

Fig. 1. XRD image of crosslinked precursor powder (a) and SiCN ceramics containing Co_3C pyrolyzed at different temperatures (b) (color online)

The crystallographic characteristics of each ceramic pyrolyzed at different temperatures were characterized by XRD pattern shown in Fig. 1(b). From the spectra, it can be seen that there was no obvious diffraction peak in the samples below 1300 ℃, indicating that the samples were mainly amorphous structures. All the samples showed the diffraction peaks of Co_3C (PDF Card No. 26-0450), indicating that cobalt particles reduced from $Co(acac)_3$ combined with C to form magnetic particles Co_3C. It is worth mentioning that the desired result is to introduce magnetic particles into SiCN ceramics to coordinate the electromagnetic parameters, so the magnetic particles Co_3C formed are satisfactory. When the pyrolysis temperature reached 1400 ℃ and above, the diffraction peaks of Si_3N_4 (PDF Card No. 33-1160) and SiC (PDF Card No. 39-1196) appeared between 32° and 36° in the XRD spectra and became sharper with the rise of temperature, indicating that the crystallization degree of the two phases increased gradually. Si_3N_4 and SiC have no magnetism [19], which may affect the absorbing properties of materials. When the pyrolysis temperature reached 1300 ℃, the characteristic peaks of C (PDF Card No. 26-1080) appeared in the XRD pattern clearly and the peak strength was enhanced with the increase of pyrolysis temperature. This indicates that the free carbon in the samples was precipitated gradually with the rise of temperature [20]. In order to reveal the existence state of carbon in the samples and the relationship between the crystallization degree of carbon and pyrolysis temperature, Raman measurements were carried out on the samples. Raman spectra and Gauss fitting data are shown in Fig. 2 and Table 1.

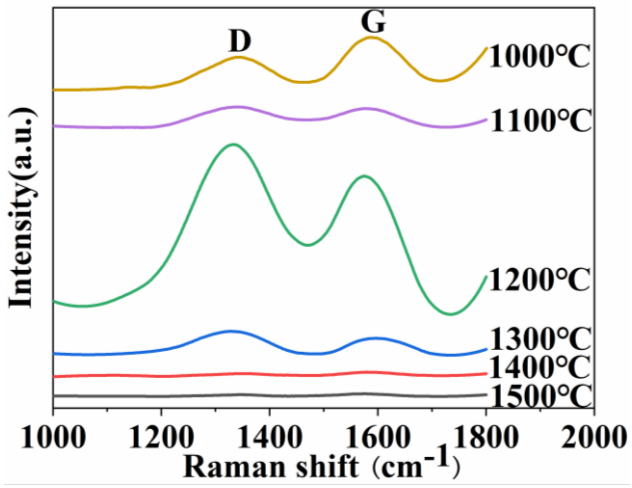

Fig. 2. Raman image of SiCN ceramics containing Co_3C pyrolyzed at different temperatures (color online)

The existence state and crystallization degree of carbon of each sample pyrolyzed at different temperatures were characterized by Raman pattern showed in Fig. 2. The D peak near the wave number 1350 cm^{-1} represents the defect of graphite lattice and the degree of structural disorder and the G peak near the wave number 1600 cm^{-1} represents the stretching vibration of carbon atom SP^2 hybridization in the graphite lattice plane [21]. All samples showed D and G peaks, illustrating that the samples pyrolyzed at different temperatures contain free carbon. Combining with XRD images, we can notice that free carbon in the samples can react with cobalt reduced from $Co(acac)_3$. In order to further explore the relationship between the crystallization degree of carbon and pyrolysis temperature, Raman data were obtained by Gaussian

fitting as shown in Table 1.

Table 1 shows the Gaussian fitting data of Raman spectra. I_D/I_G is the integral ratio of D curve to G curve, which was usually used to describe the disorder degree of free carbon in the samples; the larger the ratio of I_D/I_G, the higher the disorder degree of free carbon in the sample, that is to say, the more amorphous carbon in the sample [22-24]. From Table 1, we can see that the value of I_D/I_G increased gradually with the rise of temperature between 1000 ℃ and 1300 ℃. When the temperature was higher than 1300 ℃, I_D/I_G began to decrease with the increase of temperature. When the temperature was fixed at 1300 ℃, the maximum value of I_D/I_G was 2.063, indicating that the content of free carbon was the highest in the sample. Free carbon is a conductive phase, which will have an influence on the absorbing properties of the samples.

Table 1. Raman spectra parameters of SiCN ceramics containing Co_3C pyrolyzed at different temperatures

Temperature	I_D/I_G	$\omega_D(cm^{-1})$	$FWHH_D(cm^{-1})$	$\omega_G(cm^{-1})$	$FWHH_G(cm^{-1})$
1000℃	0.506	1340.183	89.359	1590.268	92.053
1100℃	1.401	1340.465	155.120	1576.282	124.354
1200℃	1.743	1333.272	181.670	1575.474	127.990
1300℃	2.063	1324.932	132.218	1599.460	93.723
1400℃	0.596	1348.203	100.966	1584.971	98.017
1500℃	0.578	1338.930	100.895	1572.619	106.655

3.2. Microstructure

SEM images of the cross-section morphology of samples pyrolyzed at different temperatures are shown in Fig. 3. From Fig. 3, it can be noticed that the matrix of the sample was amorphous and composed of four elements of silicon, carbon, nitrogen and oxygen (Fig. 4). Since there was no oxygen in PSZ, the oxygen may be introduced during crosslinking or pyrolysis. In addition, we can observe that bright particles were evenly distributed in the matrix. Combining with EDS element mapping of Fig. 4, it can be inferred that the bright particles were magnetic particles Co_3C. The existence of Co_3C will play a role in coordinating the electromagnetic parameters and further promoting the EMW absorption performance of the materials.

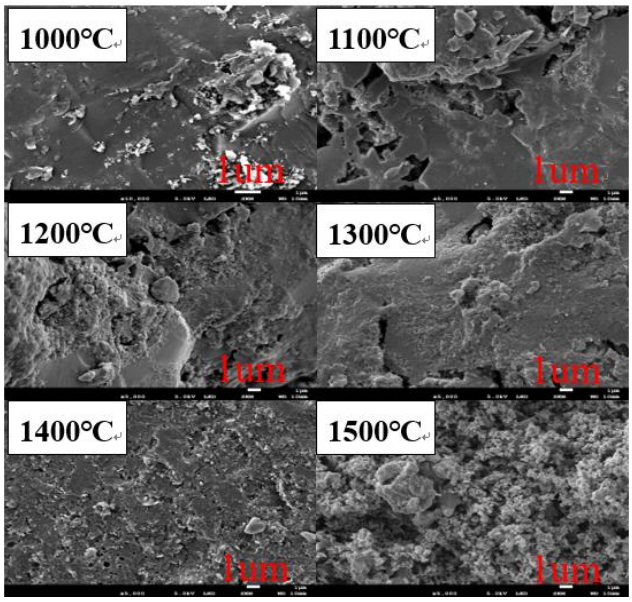

Fig. 3. SEM image of SiCN ceramics Co_3C pyrolyzed at different temperatures

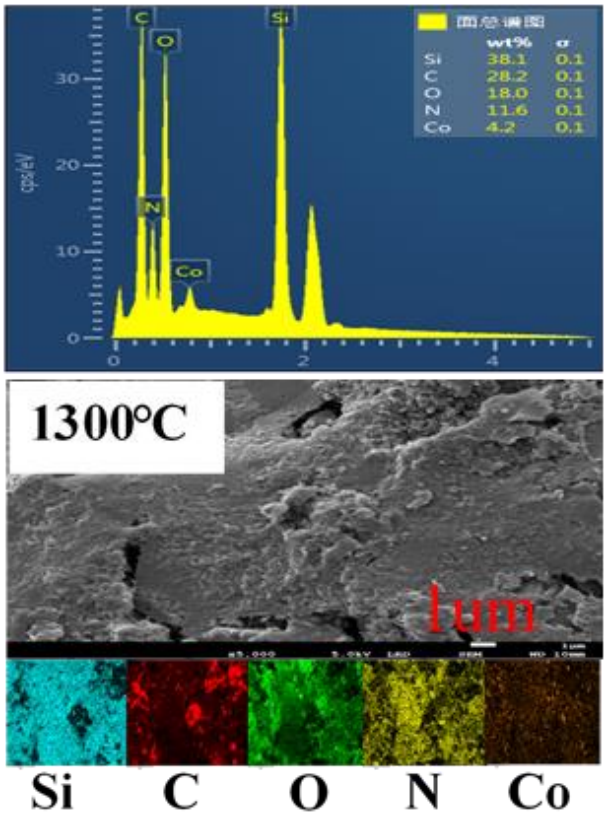

Fig. 4. EDS image of SiCN ceramics containing Co_3C pyrolyzed at 1300 ℃ (color online)

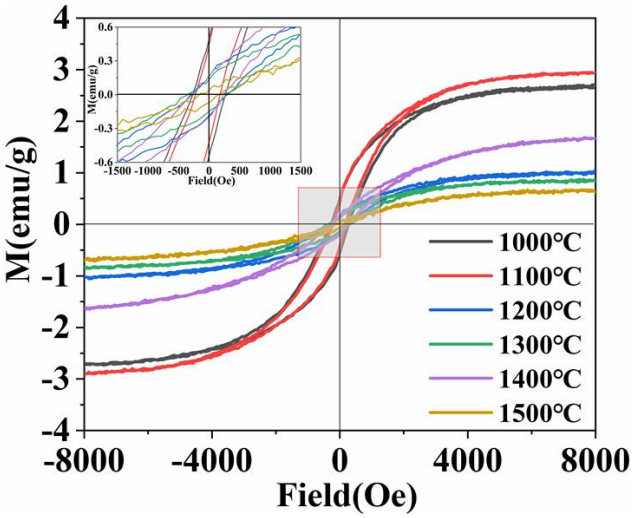

Fig. 5. Hysteresis loop of SiCN ceramics containing Co_3C pyrolyzed at different temperatures (color online)

3.3. Magnetic properties

The magnetic properties at room temperature of samples pyrolyzed at different temperatures are shown in Fig. 5. It can be clearly observed from the diagram that no matter how the pyrolysis temperature changes, the sample presents a complete hysteresis loop. SiCN ceramics are non-magnetic. Based on the analysis of XRD and SEM, we can infer that the magnetic properties of the samples came from the magnetic Co_3C particles. At the highest pyrolysis temperature (1500 ℃), the sample had the worst magnetic properties, with a saturation magnetization (Ms) of about 0.5 emu/g. Combined with the XRD analysis results, it can be inferred that this is due to the formation of a large number of non-magnetic Si_3N_4 and SiC in the samples. All samples exhibited the characteristics of soft magnetic materials (smaller Ms and coercivity). Soft magnetic materials are easy to be magnetized and demagnetized in the magnetic field. In the process of magnetization and demagnetization, part of the magnetic energy was converted into heat energy and further dissipated, thus attenuating the electromagnetic wave.

3.4. Electromagnetic characteristics

The complex permittivity ($\varepsilon_r=\varepsilon'-j\varepsilon''$) and the complex permeability ($\mu_r=\mu'-j\mu''$) are powerful parameters to characterize the electromagnetic characteristics of samples. The real (ε') and imaginary parts (ε'') of the complex permittivity and the real (μ') and imaginary parts (μ'') of the complex permeability of the sample are shown in Fig. 6 and Fig. 7. The real part represents the storage capacity of the sample for electric and magnetic energy, and the imaginary part represents the loss capacity of the sample for electric and magnetic energy [25]. Fig. 6 shows the ε' and ε'' of samples pyrolyzed at different temperatures. It can be known that the ε' decreased with the increase of frequency, which is related to the different contribution of the dipole polarization mechanism to permittivity in the AC-frequency electric field [26]. Within the range of 0-10 GHz, the fluctuation range of ε' and ε'' was small, ranging from 6-12 and 0-2, respectively. When the frequency exceeded 10 GHz, ε' and ε'' began to show higher fluctuation peaks. The fluctuation range of ε' was between 5-15, and the fluctuation range of ε'' was between -4-5. This is related to the change of polarization mechanism of ceramics in the electric field. When the sample was in the high frequency electric field, the displacement polarization of positive and negative ions between free carbon molecules disappeared, which resulted in the large fluctuation of permittivity in the high frequency electric field [27]. The sample pyrolyzed at 1500 ℃ had the lowest ε'' compared with other samples and the results of XRD analysis show that it is due to the formation of a large number of Si_3N_4 and SiC without conductivity in the samples. The sample at pyrolysis temperature of 1300 ℃ had the largest ε'' value compared with other samples, which illustrates that this sample had excellent dielectric loss ability. As we know, dielectric loss includes conductivity loss and polarization loss, while polarization loss includes electron polarization, ion polarization, dipole orientation polarization and interface polarization [28-30]. Electron polarization and ion polarization usually occur between 10^3-10^6 GHz, so they are excluded from the scope of this discussion [30]. SiCN ceramic matrix contains free carbon nanodomain, which makes it conductive [31,32]. Therefore, we speculate that the conductivity loss is one of the dielectric loss mechanisms of the prepared materials.

In addition, we can notice that ε″ fluctuated to different degrees with the increase of frequency in Fig. 6 (b). This demonstrates that the dipole in the material was unable to reorient in time to respond to the external electric field, so the polarization loss of dipole cannot be ignored [33]. In order to further explore the multiple dielectric loss mechanisms in materials, we drew an ε″- ε' image of the sample pyrolyzed at 1300 ℃, as shown in Fig. 8(a). According to Debye's theory, semicircles in the ε″- ε' image were defined as Cole-Cole semicircles, and a semicircle corresponded to a polarization relaxation process [34,35]. At least two Cole semicircles can be observed from Fig. 8(a), which proves the existence of interfacial polarization. The interfacial polarization of the prepared materials may exist between Co_3C and matrix, C and matrix [36,37]. Based on the above analysis of dielectric loss mechanism, we can speculate that the dielectric loss of the prepared materials is mainly caused by conductivity loss, dipole orientation polarization and interface polarization.

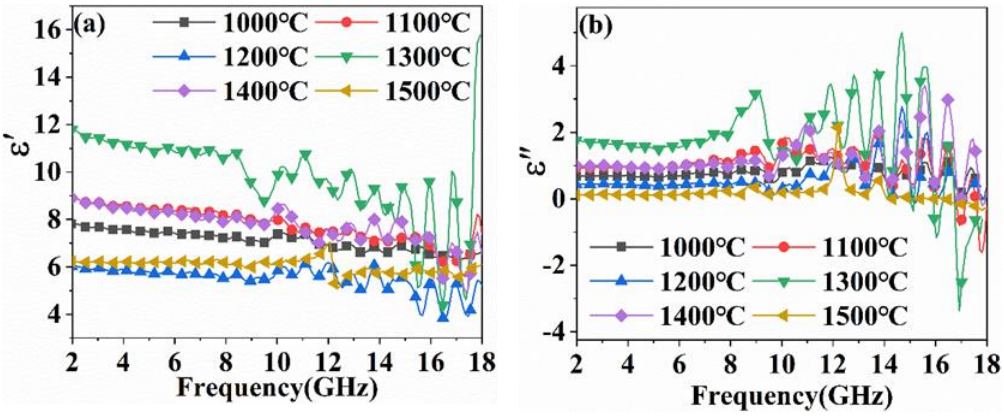

Fig. 6. Real (ε')(a) and imaginary parts (ε")(b) of permittivity of SiCN ceramics containing Co_3C pyrolyzed at different temperatures (color online)

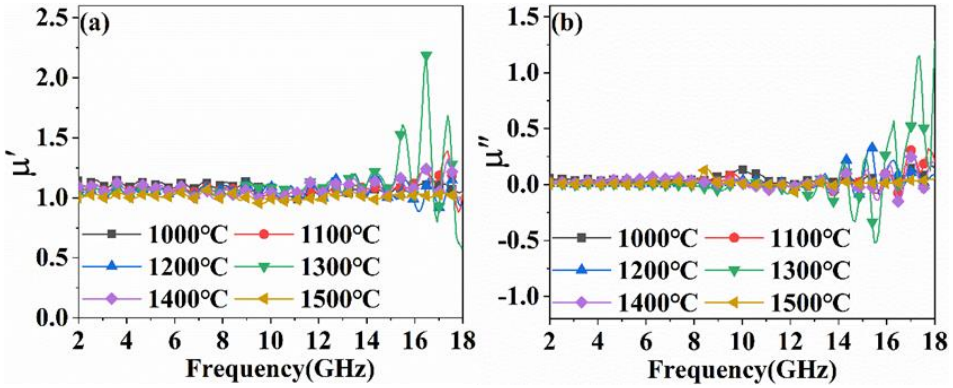

Fig. 7. Real (μ')(a) and imaginary parts (μ")(b) of permeability of SiCN ceramics containing Co_3C pyrolyzed at different temperatures (color online)

Fig. 7 shows the μ' and μ″ of samples pyrolyzed at different temperatures. Similar to ε' and ε″, the μ' of the sample had a small fluctuation range (1-1.2) in the range of 2-15 GHz. When the frequency was greater than 15 GHz, μ' began to resonate, and the data fluctuation range was enlarged. The maximum μ' and μ″ occurred in the sample pyrolyzed at 1300 ℃, showing the excellent magnetic energy storage and loss ability of this sample. We know that the magnetic energy losses include hysteresis loss, eddy current loss, natural resonance and domain wall resonance [38]. Hysteresis losses usually occur at low frequencies (1-100MHz), and domain wall resonance can be ignored in weak electromagnetic fields [39], so the magnetic loss mechanism of samples may be natural resonance and eddy current loss. In order to further determine the precise magnetic loss mechanism, we introduced the following formula [40]:

$$\mu''(\mu')^{-2}f^{-1}=2\pi\sigma d^2\mu_0 \quad (1)$$

where, d is the thickness of the sample, σ is the electric conductivity, f is the frequency, and μ_0 is the vacuum permeability. Let's take a sample pyrolyzed at 1300℃ for example. If eddy current loss is included in its magnetic

loss mechanism, no matter how the frequency changes, $\mu''(\mu')^{-2}f^{-1}$ should be a constant. However, we can clearly see from Fig. 8(b) that the value of $\mu''(\mu')^{-2}f^{-1}$ fluctuated in the range of 5-10 GHz with the change of frequency, so we can exclude the eddy current loss from the loss mechanism. Therefore, the magnetic loss of the sample is mainly caused by natural resonance.

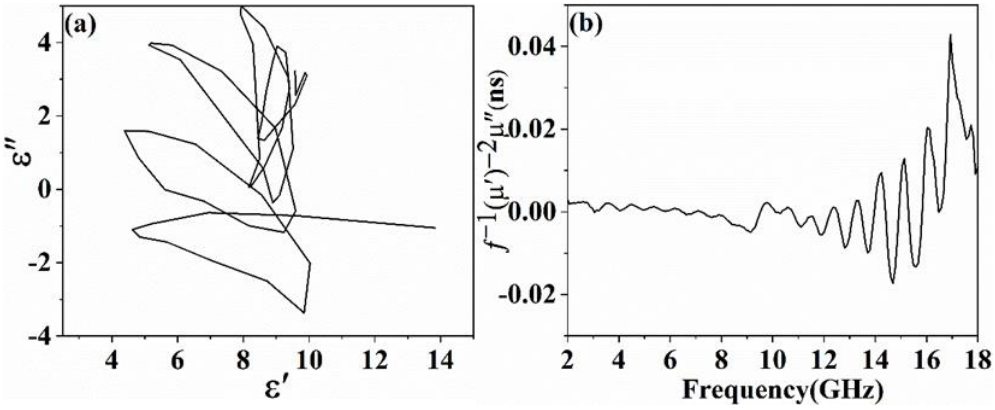

Fig. 8. Cole-Cole curves(a) and frequency dependence on $\mu''(\mu')^{-2}f^{-1}$(b) of SiCN ceramics containing Co_3C pyrolyzed at 1300 ℃

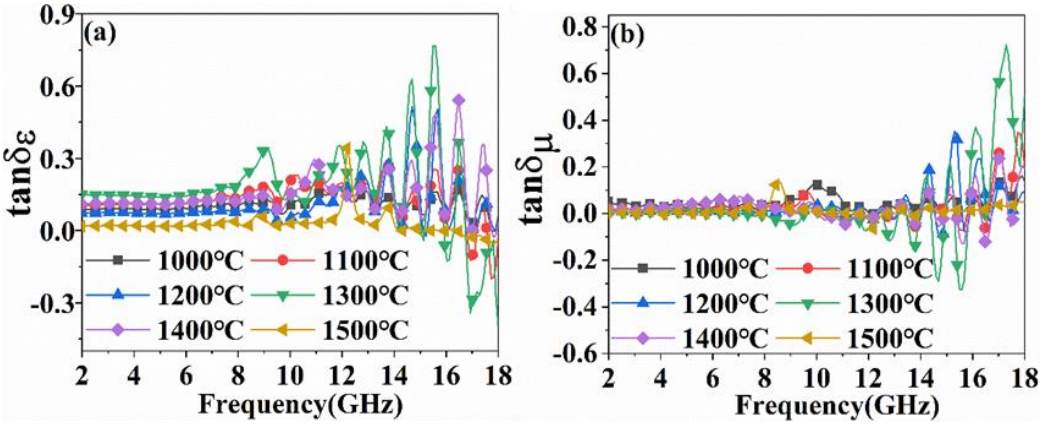

Fig. 9. Dielectric loss tangent ($tan\delta_\varepsilon$) (a) and magnetic loss tangent ($tan\delta_\mu$) (b) of SiCN ceramics containing Co_3C pyrolyzed at different temperatures (color online)

Dielectric loss tangent ($tan\delta_\varepsilon$) and magnetic loss tangent ($tan\delta_\mu$) can directly characterize the ability of the material to dissipate electromagnetic energy, which can be calculated by the following formula [41-45].

$$tan\delta_\varepsilon=\varepsilon''/\varepsilon' \quad (2)$$

$$tan\delta_\mu=\mu''/\mu' \quad (3)$$

The $tan\delta_\varepsilon$ and $tan\delta_\mu$ of the sample are shown in Fig. 9. We can find that $tan\delta_\varepsilon$ change with frequency was similar to the ε″. The maximum value of $tan\delta_\varepsilon$ appeared in the sample pyrolyzed at 1300 ℃ when frequency was about 15.5 GHz. Similarly, $tan\delta_\mu$ change with frequency was similar to μ″. The maximum value of $tan\delta_\mu$ appeared in the sample pyrolyzed at 1300 ℃ when frequency was about 17.4 GHz. By comparing the two images of $tan\delta_\varepsilon$ and $tan\delta_\mu$, we can find that they had approximate values at various frequencies, which indicates that the EMW absorption performance of the sample is accomplished by the coordination of dielectric loss and magnetic energy loss.

3.5. Microwave absorption performance

Based on the transmission line theory, the reflection loss (RL) of the sample can be calculated by the following formula [46-48]:

$$R_L\,(dB)=20\log|(Z_{in}-1)/(Z_{in}+1)| \quad (4)$$

$$Z_{in}/Z_0=(\mu_r/\varepsilon_r)^{1/2}\tanh[j(2\pi/c)fd(\varepsilon_r\mu_r)^{1/2}] \quad (5)$$

where, Z_{in} is the input impedance of the material surface, ε_r and μ_r are the complex permittivity and complex permeability, c is the speed of light, d is the thickness of the sample, f is the frequency, and R_L < -10dB means that more than 90% of the EMW is absorbed. Fig. 10(a) shows the R_L of the crosslinked precursor powder. It can be seen from the figure that the EMW absorption properties of

precursor powder are unsatisfactory. The optimum R_L can only reach -9 dB, and the effective absorption bandwidth (EAB, R_L < -10dB) was 0. Fig. 10(b) shows the R_L of ceramics obtained from the precursor powder pyrolyzed at different temperatures. According to the image, we can notice that with the increase of frequency, the EMW absorption performance of samples became superior. Particularly, the sample pyrolyzed at 1300 ℃ exhibited the best EMW absorption properties. It can be observed in Fig. 10(b) that when the thickness was 2 mm, R_L achieved an optimum value –14 dB at 16.5 GHz, and the EAB was 0.6 GHz, showing excellent EMW absorption efficiency. In addition, the EMW absorption rate of the sample pyrolyzed at 1200 ℃ reached 87% (R_L<-9 dB), showing good performance.

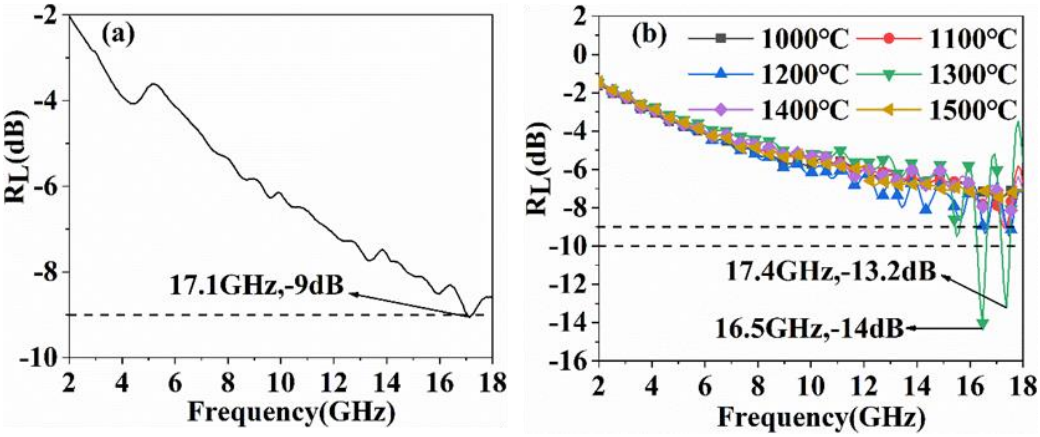

Fig. 10. Reflection loss (R_L) of crosslinked precursors (a) and SiCN ceramics containing Co_3C pyrolyzed at different temperatures (b) (color online)

In order to investigate the variation regularity of EMW absorption properties with sample thickness, we made R_L curves (a) and 3D plots (b) of SiCN composite ceramics pyrolyzed at 1300 ℃ at different thickness. According to Fig. 11, we can observe that R_L decreased gradually with the increase of sample thickness in the range of 2-8 GHz. When the frequency was greater than 8 GHz and the thickness of the sample exceeded 3 mm, there was no significant change in the R_L values. When the thickness of the sample reached 6 mm, the EAB was still 0.6 GHz, but the R_{Lmin} achieved -14.5 dB, which proves that the absorbing properties of the sample will change with the thickness and we can adjust the desired absorption efficiency by controlling the sample thickness.

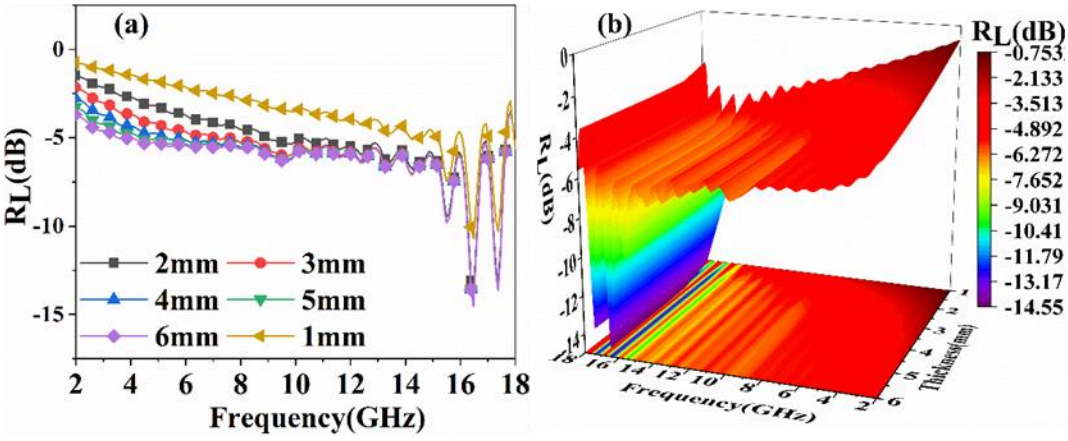

Fig. 11. R_L curves(a) and 3D plots(b) of SiCN ceramics containing Co_3C pyrolyzed at 1300 ℃ at different thickness (color online)

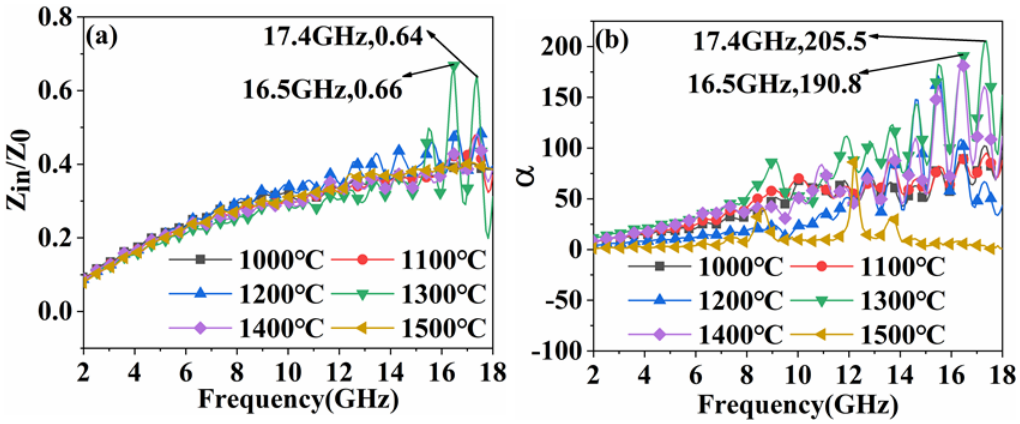

Fig. 12. Impedance matching parameters (Z_{in}/Z_0) (a) and electromagnetic attenuation coefficient (α)(b) of SiCN ceramics containing Co_3C pyrolyzed at different temperatures (color online)

Impedance matching parameter (Z_{in}/Z_0) and attenuation coefficient (α) were recognized to affect the absorption performance and their calculation formulas were the formula 5 and the formula 6, respectively [49]. Impedance matching refers to the matching between material impedance and free space impedance. The closer the value of Z_{in}/Z_0 is to 1, the better the EMW absorbing function of the material. We drew the Z_{in}/Z_0 images of each sample obtained, as shown in Fig. 12. From Fig. 12(a), we can be aware of that when the frequency was 16.5 GHz and 17.4 GHz, the sample pyrolyzed at 1300 ℃ had the highest impedance matching with air compared with other samples. The results show that the samples pyrolyzed at this temperature can make the incident EMW enter the interior of the material to the maximum extent when the frequency was 16.5 GHz and 17.4 GHz. α represents the ability of materials to convert the electromagnetic energy into other forms of energy and further dissipate them. The larger the value is, the stronger the wave attenuation ability of the material is. Fig. 12(b) exhibits the α of each sample. We can see from Fig. 12(b) that, similar to Z_{in}/Z_0, when the frequency was 16.5 GHz and 17.4 GHz, the samples pyrolyzed at 1300 ℃ had the largest α. This result demonstrates that at the two frequencies, the sample pyrolyzed at 1300 ℃ had the strongest EMW attenuation ability. By the analysis of Z_{in}/Z_0 and α above, we can conclude that when the frequency was 16.5 GHz and 17.4 GHz and the pyrolysis temperature was 1300 ℃, the material can make the incident EMW enter into its interior as far as possible and further attenuate them. Therefore, excellent impedance matching and wave attenuation function together determine the superb EMW absorption properties of the material.

$$\alpha=(\pi f/c)\,.(\mu'\varepsilon')^{½}\,.\,[(\tan\delta_{\varepsilon}.\tan\delta_{\mu}-1)+(\tan^2\delta_{\varepsilon}+1)^{½}.(\tan^2\delta_{\mu}+1)^{½}]^{½} \quad (6)$$

Based on the above analysis, the excellent EMW absorption performance of as-prepared composite ceramics is the result of the coordination and interaction of various loss mechanisms, rather than the dominant result of a single mechanism. Firstly, the free carbon nanodomains in the SiCN ceramic matrix can promote the electron transport. Conductive loss is formed during the process of electron movement in which part of the electrical energy is converted into heat energy and further dissipated. Secondly, magnetic Co_3C particles produce magnetic energy loss due to natural resonance in the magnetic field. Finally, the polarization loss is caused by the rotation of the dipole in the alternating electromagnetic field and the interface polarization between different phases. A variety of loss mechanisms coordinate with each other and work together to contribute to excellent EMW absorption properties of the composite ceramics.

4. Conclusion

Polymer-derived SiCN ceramics doped with Co_3C particles were prepared in this study. On this basis, the phase composition and microstructures of samples pyrolyzed at different temperatures were tested. The electromagnetic characteristic and the EMW absorption performance at 2-18 GHz were studied. The results show that cobalt was reduced from $Co(acac)_3$ during the crosslinking process, and then reacted with carbon to form magnetic particles Co_3C during the pyrolysis procedure, which makes the sample magnetic. The sample has excellent EMW absorption performance due to the electromagnetic synergic effect. When the pyrolysis temperature was fixed at 1300 ℃ and the thickness of the sample was 2 mm, the R_{Lmin} reached -14dB, and the EAB was 0.6 GHz. With the increase of sample thickness, the R_L decreased. When the sample thickness was 6 mm, the R_{Lmin} was - 14.5 dB, and the EAB was 0.6 GHz. This indicates that polymer-derived SiCN ceramics doped with Co_3C have excellent EMW absorption properties and can be used as one of the candidates for EMW absorbing materials.

Acknowledgment

This work was financed by the National Science

Foundation of China (No.51572154).

References

[1] Girgert, Rainer et al., Bioelectromagnetics: Journal of the Bioelectromagnetics Society, The Society for Physical Regulation in Biology and Medicine, The European Bioelectromagnetics Association **29.3**, 169 (2008).
[2] X. G. Liu, J. J. Jiang, D. Y. Geng et al., Applied Physics Letters **94**(5), 053119 (2009).
[3] Y. Wang, T. Li, L. Zhao et al., Energy and Power Engineering **3**(04), 580 (2011).
[4] F. Qin, H. X. Peng, Progress in Materials Science **58**(2), 183 (2013).
[5] W. Duan, X. Yin, Q. Li et al., Journal of the European Ceramic Society **36**(15), 3681 (2016).
[6] Y. Zhang, Y. Huang, T. Zhang et al., Advanced Materials **27**(12) 2049 (2015).
[7] X. Guo, Y. Feng, X. Lin et al., Journal of the European Ceramic Society **38**(4), 1327 (2018).
[8] Y. Feng, X. Guo, H. Gong et al., Ceramics International **44**(9), 10420 (2018).
[9] Y. Liu, X. Lin, H. Gong et al., Journal of Alloys and Compounds **771**, 356 (2019).
[10] Y. Liu, Y. Feng, H. Gong et al., Advanced Functional Materials. Chinese Materials Conference. Springer, Singapore, 83 (2017).
[11] Y. Liu, Y. Feng, H. Gong et al., Journal of Materials Science: Materials in Electronics **29**(14), 12496 (2018).
[12] N. Li, C. Hu, M. Cao, Physical Chemistry Chemical Physics **15**(20), 7685 (2013).
[13] G. V. Kurlyandskaya, S. M. Bhagat, C. Luna et al., Journal of Applied Physics **99**(10), 104308 (2006).
[14] P. Toneguzzo, G. Viau, O. Acher et al., Advanced Materials **10**(13), 1032 (1998).
[15] J. Zhang, P. Wang, Y. Chen et al., Journal of Electronic Materials **47**(8), 4703 (2018).
[16] X. Qi, Q. Hu, H. Cai et al., Scientific Reports **6**, 37972 (2016).
[17] I. Abdalla, J. Shen, J. Yu et al., Scientific Reports **8**(1), 12402 (2018).
[18] J. Xiang, J. Li, X. Zhang et al., J. Mater. Chem. A **2**(40), 16905 (2014).
[19] P. Colombo, R. Riedel, G. D. Sorarù et al., DEStech Publictions Inc., Lancaster, PA 1-12 (2009).
[20] L. Li, L. Cheng, S. Fan et al., Journal of Alloys and Compounds **656**, 654 (2016).
[21] X. Wang, M. Yu, W. Zhang et al., Applied Physics A **118**(3), 1053 (2015).
[22] X. Sun, J. He, G. Li et al., Journal of Materials Chemistry C **1**(4), 765 (2013).
[23] A. C. Ferrari, J. Robertson, Physical Review B **64**(7), 075414 (2001).
[24] N. Janakiraman, F. Aldinger, J. Eur. Ceram. Soc. **29**, 163 (2009).
[25] Y. Lü, Y. Wang, H. Li et al., ACS Applied Materials & Interfaces **7**(24), 13604 (2015).
[26] F. Ye, L. Zhang, X. Yin et al., Journal of the European Ceramic Society **33**(8), 1469 (2013).
[27] X. Guo, Y. Feng, Y. Liu et al., Ceramics International **43**(18), 16866 (2017).
[28] B. Wen, M. S. Cao, Z. L. Hou et al., Carbon **65**, 124 (2013).
[29] M. M. Lu, W. Q. Cao, H. L. Shi et al., Journal of Materials Chemistry A **2**(27), 10540 (2014).
[30] C. Tian, Y. Du, P. Xu et al., ACS Applied Materials & Interfaces **7**(36), 20090 (2015).
[31] Q. Li, X. Yin, W. Duan et al., Journal of the European Ceramic Society **34**(3), 589 (2014).
[32] B. N. Sahoo, B. Choi, J. Seo et al., Journal of Semiconductors **39**(1), 011009 (2018).
[33] A. Ohlan, K. Singh, A. Chandra et al., ACS Applied Materials & Interfaces **2**(3), 927 (2010).
[34] F. Yu, H. Deng, Q. Zhang et al., Polymer **54**(23), 6425 (2013).
[35] D. Lan, M. Qin, J. Liu et al., Chemical Engineering Journal **382**, 122797 (2020).
[36] M. Cao, X. Wang, W. Cao et al., Small **14**(29), 1800987 (2018).
[37] H. J. Yang, W. Q. Cao, D. Q. Zhang et al., ACS Applied Materials & Interfaces **7**(13), 7073 (2015).
[38] H. Wang, Z. Yan, J. An et al., RSC Advances **6**(95), 92152 (2016).
[39] M. Wu, Y. D. Zhang, S. Hui et al., Applied Physics Letters **80**(23), 4404 (2002).
[40] D. Li, Y. Feng, D. S. Pan et al., RSC Advances **6**(77), 73020 (2016).
[41] Q. Liu, Q. Cao, X. Zhao et al., ACS Applied Materials & Interfaces **7**(7), 4233 (2015).
[42] Q. Su, J. Li, G. Zhong et al., The Journal of Physical Chemistry C **115**(5), 1838 (2011).
[43] G. Li, T. Xie, S. Yang et al., The Journal of Physical Chemistry C **116**(16), 9196 (2012).
[44] C. Yan, X. Cheng, Y. Zhang et al., The Journal of Physical Chemistry C **116**(49), 26006 (2012).
[45] Y. J. Chen, F. Zhang, G. Zhao et al., The Journal of Physical Chemistry C **114**(20), 9239 (2010).
[46] H. Nikmanesh, M. Moradi, G. H. Bordbar et al., Journal of Alloys and Compounds **708**, 99 (2017).
[47] S. Chang, S. Kangning, C. Pengfei, Journal of Magnetism and Magnetic Materials **324**(5), 802 (2012).
[48] Z. Zhang, X. Liu, X. Wang et al., Journal of Alloys and Compounds **525**, 114 (2012).
[49] B. Zhao, G. Shao, B. Fan et al., Physical Chemistry Chemical Physics **17**(14), 8802-10 (2015).

*Corresponding author: gong_hongyu@163.com